DOE/ER/10433-2

Annual Technical Progress Report II

A MICROSTRUCTURAL APPROACH TO FATIGUE CRACK PROCESSES IN POLYCRYSTALLINE BCC MATERIALS

by

William W. Gerberich

Department of Chemical Engineering and Materials Science
Univeristy of Minnesota
Minneapolis, MN 55455

Submitted to Basic Energy Sciences, DOE

Attention: Dr. Stanley Wolf

April 1, 1981

EAB

DISCLAIMER

TABLE OF CONTENTS

PROGRAM OBJECTIVES AND SUMMARY

Little is known about what controls fatigue cracking near threshold in BCC materials. Furthermore, although these are acceptable models of plastic flow induced striation mechanisms, there are no generally accepted models involving intergranular, cleavage, cyclic cleavage, glide band decohesion or other secondary fracture modes. The objectives of the present program are to understand the roles of alloy additions, grain size and yield strength on fatigue threshold and near-threshold growth rates for selected BCC materials. Thus far, a predictive model for burst cleavage in Fe-binary alloys has been derived and verified. A predictive model for cyclic strain hardening exponents of an HSLA steel at low temperatures has been derived and verified. A proposed model for cyclic cleavage crack entension in terms of geometrically mecessary dislocations has been partially investigated. Experimentally, grain size and low temperature effects on thresholds and crack growth of HSLA steels and Ti-30 Mo have been nearly completed and similar studies on Fe-binary alloys are in progress. With such input, models are currently being developed for prediction of microstructural effects on threshold and near-threshold crack growth under mixed mode conditions.

I. STRAIN-RATE SENSITIVITY AND DISLOCATION DYNAMICS

As was indicated in the first year's Progress Report,[1] there were some basic needs of understanding the grain size effect on strain rate sensitivity if dislocation dynamics were going to be utilized to model the plastic rate equation appropriate to the crack tip. These needs were prompted by some standard thermal activation analysis on HSLA steel where m^* was defined as usual from

$$\dot{\varepsilon} = \rho_m b v_o \left(\frac{\sigma^*}{\sigma}\right)^{m^*} \tag{1}$$

Upon differentiating and assuming ρ_m is constant, this gives

$$m^* = \partial \ell n \dot{\varepsilon} / \partial \ell n \sigma^* \tag{2}$$

However, the values determined in this manner from change of strain-rate testing, as recalled from the initial report and shown in Figure 1, demonstrated a grain size dependency. These have been verified with double strain-rate cycling and are known not to be dependent, entirely, on solute concentration differences.† It is more likely that such changes are an apparent effect which may be reflecting actual changes in mobile dislocation density, as previously suggested.[1,6] In fact, we will show that there could be two sources of error in current approaches. One is associated with assuming a constant mobile dislocation density and the other has to do with ignoring the time rate of variation of total dislocation density. Without going into detail, it is suggested that

$$m^*_{real} = \frac{\partial \ell n \left(\dot{\varepsilon} - \frac{d\rho}{dt} \frac{b}{2\rho^{\frac{1}{2}}}\right)}{\partial \ell n \sigma^*} - \frac{\partial \ell n \rho_m}{\partial \ell n \sigma^*} \tag{3}$$

Since $d\rho/dt$ and ρ_m are likely to be functions of stress, it follows that m^*_{real} may be substantially smaller than m^* from Eq. (2). All this analysis

---

†The amount of Nb or C in solid solution could be slightly different in the finest grain size material but imperceptibly different in the three coarsest grain sizes.

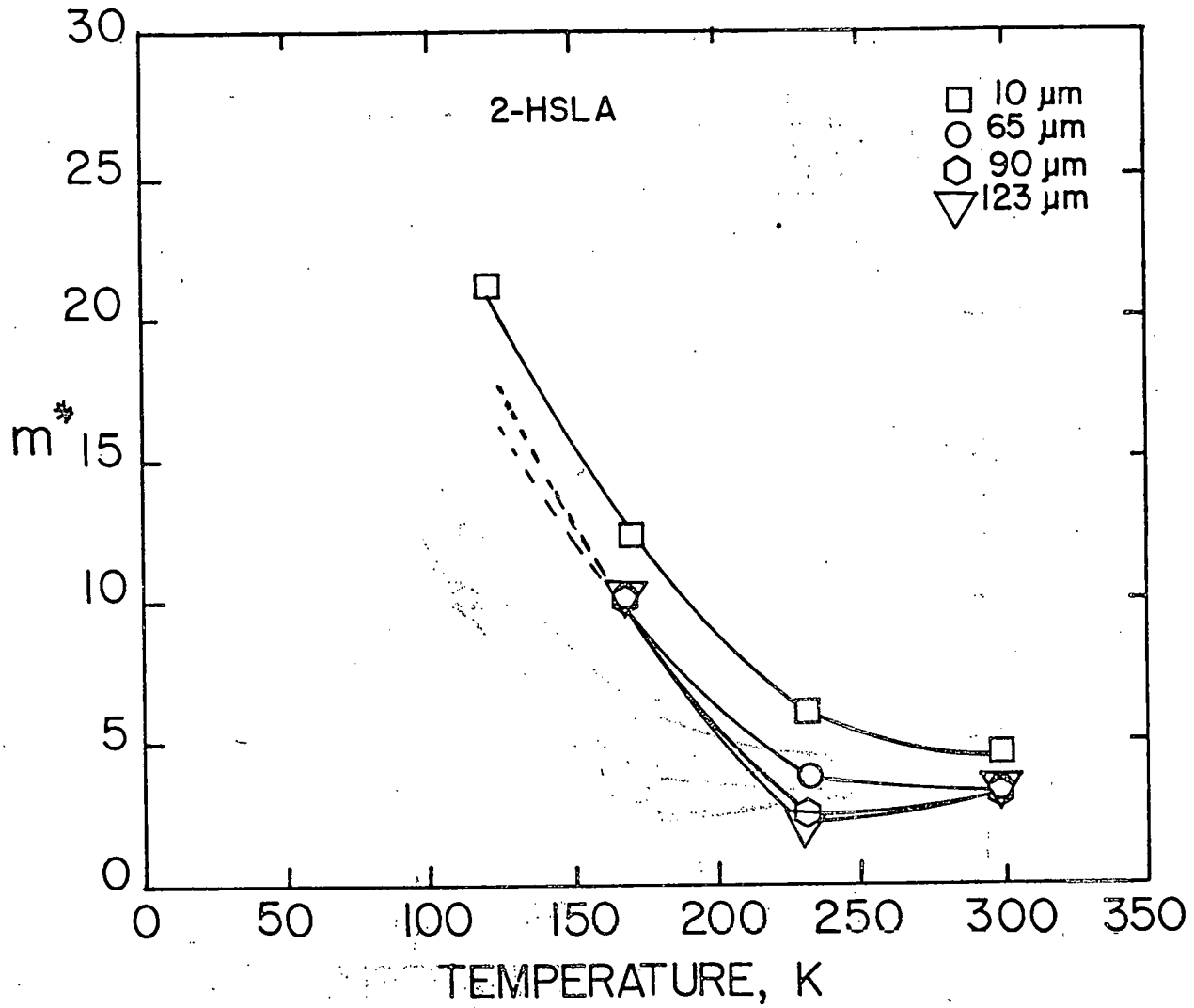
2-HSLA
10 μm
65 μm
90 μm
123 μm
m*
30
25
20
15
10
5
0
0
50
100
150
200
250
300
350
TEMPERATURE, K

Figure 1

says is that the more the strain rate is made up by dislocation creation (e.g. emissary dislocations from grain boundaries) during a strain-rate change, the less need there is for a large m^* exponent. In fact, for realistic values of dislocation density on the order of $10^{13}/m^2$, one can demonstrate that a factor of three increase in $d\rho/dt$ can result in m^*_{real} being less than half $m^*_{apparent}$. Since one would expect $d\rho/dt$ to increase as the grain size decreases, this qualitative observation is in the right direction and may at least partially explain the results in Figure 1.

Current progress in this area involves preparation of the Fe-binary alloys for thermal activation studies, stress-relaxation testing and internal stress evaluation of Ti-gettered iron and recovery experiments on both HSLA steel and iron. Over the last year, two graduate studnets (James Lucas and John Vasatis) have been involved in this phase of the research.

I-1 Consistent stress relaxation, stress recovery and positive-negative internal stress determination.

James Lucas, John Vasatis and William Gerberich

In the present dislocation dynamics, low cycle fatigue and fatigue crack propagation studies at low temperatures, it is necessary to know how the internal stress state is changing. That is how does the internal stress state change with time due to dislocation production and/or annilihation in conjunction with changes in dislocation velocity? This has caused us considerable concern since we have observed that the internal stress determined by decremental unloading is a function of the relaxation time in HSLA steels. Such a result is shown in Figure 2 where a stress-relaxation test was periodically unloaded to determine the internal stress by decremental unloading. As is seen by the inserted tabulation, the internal stress decreased by seven percent in this relatively short time (short considering the temperature of 173K where relaxation is sluggish.) Thus, there is some question as to how

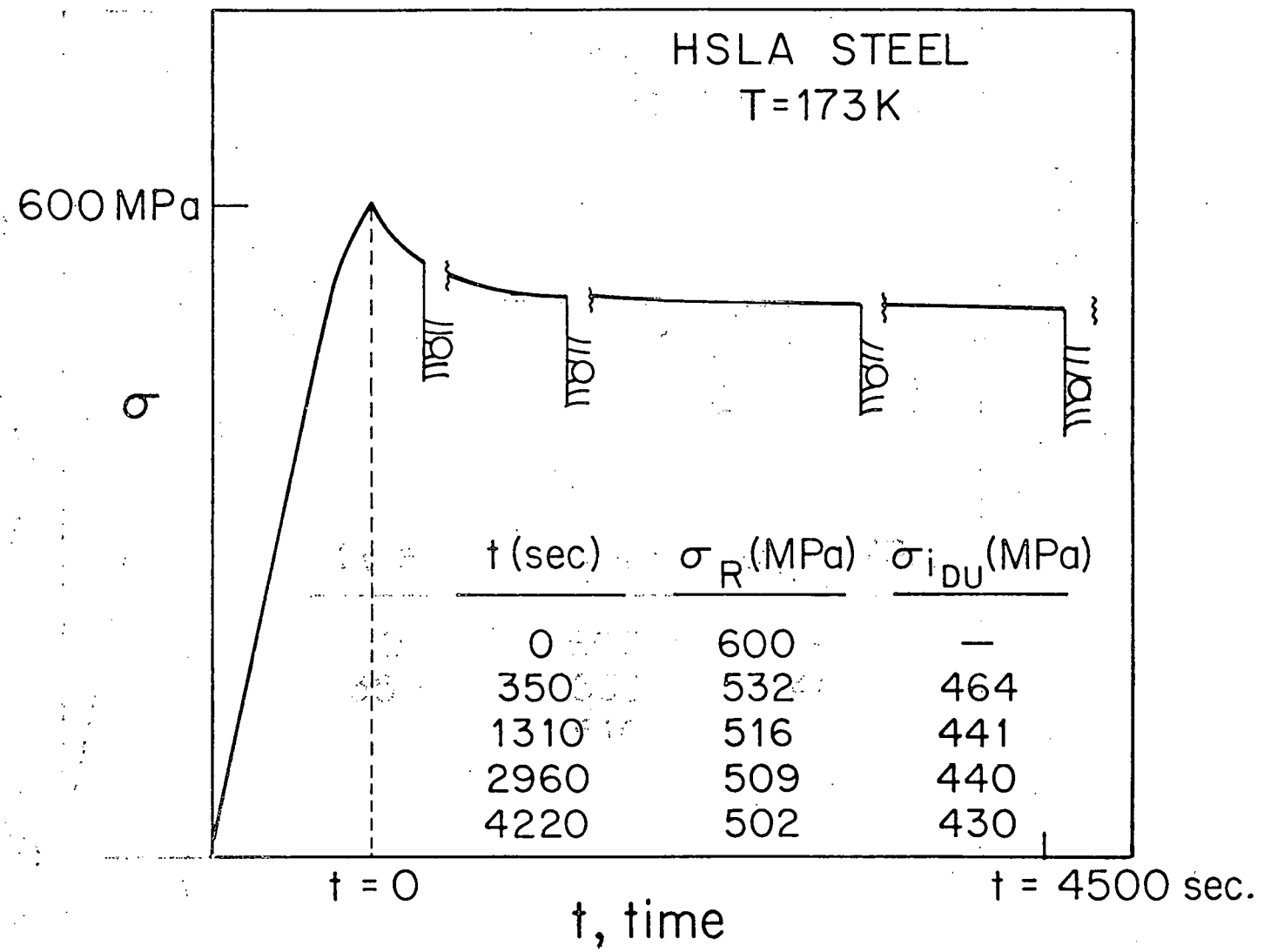
HSLA STEEL
T=173K
600 MPa
σ
t (sec)
σ_R (MPa)
σ_i DU (MPa)
0 600 —
350 532 464
1310 516 441
2960 509 440
4220 502 430
t = 0
t = 4500 sec.
t, time

Figure 2

to assess the internal stress and hence the thermal component of the flow stress.

Since the primary concern is with threshold stress intensities which will result in long time cycling at this temperature and above, the time dependence of the internal stress is important. In addition, the stress distribution at the crack tip is both large near it and small far away so that stress relaxation and/or recovery under static loads is possible. Of course, it is the cyclic loads that are of ultimate concern but for this initial study, a detailed analysis of stress relaxation and recovery under static loads is appropriate.

Consider first what happens in a stress relaxation or unloading type test. This is shown by the schematic in Figure 3 where the first test is a normal stress relaxation test, the next two represent low stress recovery experiments and the final two represent low stress recovery experiments. At high stresses, the force on the dislocations is sufficient to maintain positive dislocation motion and creation in excess of annihilation so that the specimen continues to lengthen, giving a relaxation under fixed grip conditions. At low stresses, however, a reverse condition of negative dislocation motion and/or annihilation causes a specimen shortening with an attendant stress recovery. This later condition is depicted in the schematic.

To model this, consider fixed grip stress relaxation under low stresses so that we may ignore machine relaxation. It is known that the displacement change is zero. Likewise, the total strain rate must be a balance between plastic and elastic relaxation rates, i.e.

$$\dot{\varepsilon}_{total} = \dot{\varepsilon}_E + \dot{\varepsilon}_p = 0 \qquad (4)$$

The sign of ε_E and ε_p depend upon whether the stress is large enough to overcome the instantaneous internal stress so that positive or negative relaxation occurs. This will be interpreted in terms of dislocation dynamics as others

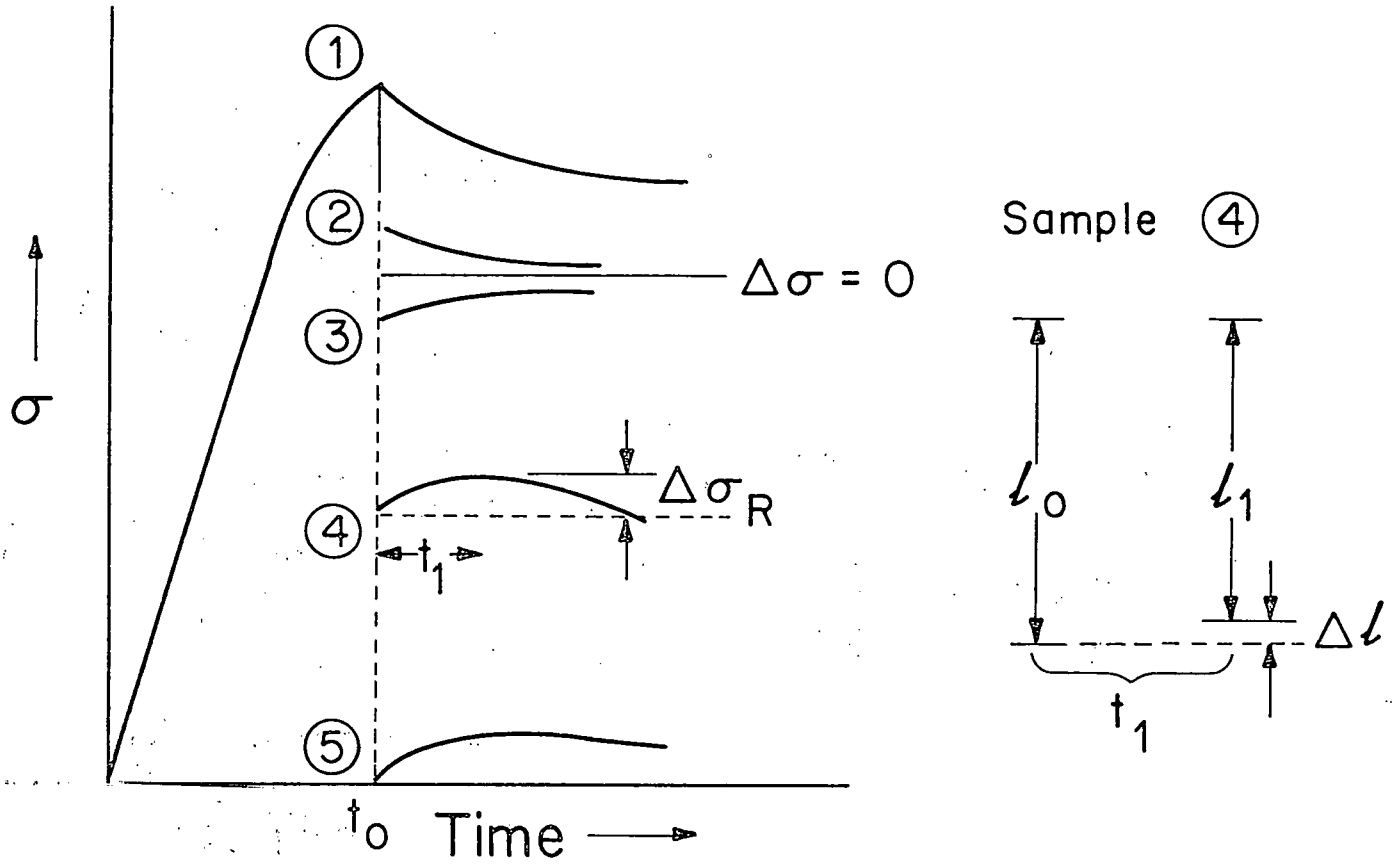

Figure 3

have done.[2-4] The plastic strain is given in terms of the dislocation density, ρ, and the average distance moved, $\bar{s}$, by

$$\varepsilon_p = \rho b \bar{s} \tag{5}$$

Both time rate of dislocation motion and generation should be considered for the plastic strain rate giving

$$\dot{\varepsilon}_p = \phi \dot{\rho}(t) b \bar{s} + \phi \rho_m(t) b \dot{\bar{s}} \tag{6}$$

where ϕ is an orientation factor.

This is essentially the same equation used by Meyers, et al[5] except that here $\rho(t)$ and $\rho_m(t)$ are not taken to be synomynous. This is necessary because the created or annihilated population may be significantly different than the mobile population. This did not create a problem for Myers, et al[5] since they only considered relaxation at high stresses where the velocity term predominates. However, for generality, both terms will be kept here. In a stress relaxation or recovery experiment, the elastic strain rate is given by

$$\dot{\varepsilon}_E = \frac{1}{E} \frac{d\sigma}{dt} \tag{7}$$

For $\bar{s}$ and $\dot{\bar{s}}$, the following are assumed

$$\bar{s} \simeq \frac{1}{2\rho^{\frac{1}{2}}} \quad ; \quad \dot{\bar{s}} = \bar{v} = v_o \left(\frac{\sigma^*}{\sigma_o}\right)^{m^*} \tag{8}$$

These parameters need only slight explanation since the empirical equation for dislocation velocity, $\bar{v}$, is well known with $m^* = \partial \ell n \dot{\varepsilon} / \partial \ell n \sigma^*$ and σ_o the stress at which the dislocation velocity is v_o. The average distance moved by each dislocation is taken as half the average distance between them since two dislocations may move half way between barriers and annihilate, a moving dislocation may annihilate a stored dislocation or a created dislocation may be immediately stored. Combining Eqs. (4), (6), (7) and (8) gives

$$\frac{1}{E} \frac{d\sigma}{dt} = - \frac{d\rho(t)}{dt} \frac{b}{2\{\rho(t)\}^{\frac{1}{2}}} - \rho_m(t) b v_o \left(\frac{\sigma^*}{\sigma_o}\right)^{m^*} \tag{9}$$

Even with the implicit assumption that the thermal component of the flow stress is constant, independent of time, this is a very complicated differential equation. An attempt to simplify it was made by choosing realistic time-dependent functions for $\rho(t)$ and $\rho_m(t)$. The time dependent variation in dislocation density proposed by Meyers, et al[5] can be closely modelled by †

$$\rho_m = 2\beta e^{-t/t_o} \tag{10}$$

where β is a constant having dislocation density units. Not only does this fit their short time data but it also gives ρ_m to be zero at infinite time, i.e. after complete relaxation. An analagous equation for the total dislocation density is

$$\rho = \beta[1 + e^{-t/t_o}] \tag{11}$$

This is realistic since it is finite at infinite time and is always greater than ρ_m. Using Eqs. (9-11) and separating veriables leads to

$$\int_{\sigma_1}^{\sigma_2} d\sigma = \int_o^t \frac{Eb\beta^{\frac{1}{2}}e^{-t/t_o}}{t_o[1+e^{-t/t_o}]^{\frac{1}{2}}}\, dt - \int_o^t 2b\beta e^{-t/t_o}\, v_o \left(\frac{\sigma^*}{\sigma_o}\right)^{\dot{m}^*} E dt \tag{12}$$

Upon integration, this gives

$$\Delta\sigma = Eb\beta^{\frac{1}{2}}\, 2^{\frac{1}{2}} - [1+e^{-t/t_o}]^{\frac{1}{2}} \; - 2\beta t_o[1-e^{-t/t_o}]bEv_o \left(\frac{\sigma^*}{\sigma_o}\right)^{m^*} \tag{13}$$

This appears to have many of the features required to model stress relaxation and recovery phenomena. A critical experiment was to examine the $\Delta\sigma_R$ transients at lower stresses where both terms were important. This was accomplished by evaluating stress recovery at short times after decremental unloading. The $\Delta\sigma_R$ after 90 seconds of recovery were measured as schematically shown in Figure 3. As is shown in Figure 4, the $\Delta\sigma_R$ values first increased and then decreased with increased values of the decremental unloading stress. The largest recovery occurred near a stress of 69 MPa which is the reported value of the internal stress for pure Fe.[6] This behavior was observed for 300 and 233 K

† There is no reason to expect that Ti-gettered iron or HSLA steels of this study will have the same exponential dependence as was observed by Meyers, et al[5] for Armco Fe.

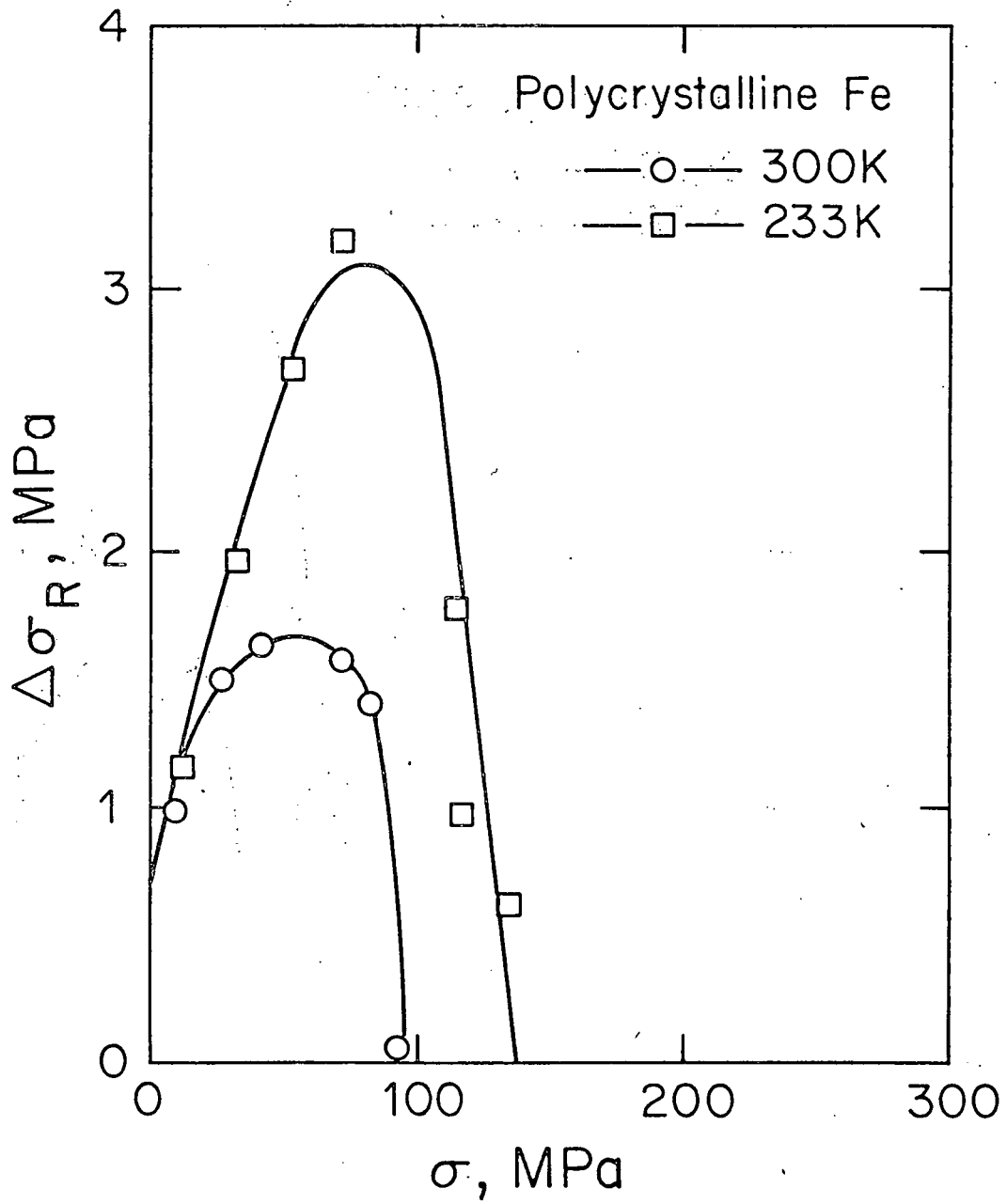
Polycrystalline Fe
300K
233K
$\Delta\sigma_R$, MPa
σ, MPa
0
1
2
3
4
0
100
200
300

Figure 4

tests as well as for 173 K (not shown here). Although Eq. (13) can model such behavior for stresses greater than σ_i it cannot for stresses less than σ_i. That is, there is no parameter which allows $\Delta\sigma_R$ to increase with an increase of the unloading stress, i.e. the stress at which recovery is initiated. There are probably several reasons for the physical inadequacy. First, there is no reason to expect all dislocations to be mobile dislocations immediately upon unloading, which is what Eqs. (10) and (11) infer. Secondly, there is good reason to expect the mobile and total dislocation density densities to be some function of stress. There is also a concern about the conservation of dislocations since annihilation, creation and stored dislocations have been inadequately treated. Such a treatment will be discussed in the proposed work for next year.

I-2 Strain-rate and flow sensitive properties of HSLA steels

James Lucas and William W. Gerberich

Besides the strain rate sensitivity, internal stress and stress recovery data already mentioned, we have been performing some stress relaxation experiments at ambient and low temperatures. These will be reported at a later date. In addition, all of the static and cyclic strain-hardening flow properties have been determined for the HSLA steels reported in Table I-1.

Table I-1: Composition of HSLA Steels (wt.%)

	C	Nb	Mn	Fe	
Heat #1	0.06	0.03	0.35	bal	RET*
Heat #2	0.06	0.03	0.35	bal	non-RET
Heat #3	0.06	0.12	1.00	bal	non-RET

*Rare-earth treated.

The cyclic strain-hardening properties are fully reported in section II-1.

References (Section I)

1. W.W. Gerberich, "A Microstructural Approach to Fatigue Crack Processes in Polycrystalline BCC Materials," Annual Technical Progress Report I, University of Minnesota, Minneapolis, April 1, 1980.

2. J.C.M. Li, Can. J. Phys., 45 (1967) p. 493.

3. U.F. Kocks, in Constitution Equations in Plasticity, p. 81 (ed. by A.S. Argon), The MIT Press, Cambridge, MA (1975).

4. E.W. Hart, C.Y. Li, H. Yamada and G.L. Wire, ibid., p. 149.

5. M.A. Meyers, J.R.C. Guimarães and R.R. Avillez, Met. Trans., 10A (January 1979) p. 33.

6. Y.T. Chen, D.G. Atteridge and W.W. Gerberich, "Dislocation Dynamics of Fe-binary Alloys: I. Low Temperature Plastic Flow," accepted for publication, Acta Metallurgica (1981).

II. FATIGUE AND FRACTURE CHARACTERIZATION

For analysis of fatigue propagation models, particularly at low temperatures, cyclic strain-hardening exponents, cyclic cleavage planes and cleavage stresses must be determined. The first year's effort was mainly centered on improving the cylic stress-strain technique, using the HSLA steels. This second year's progress has involved the complete characterization of one HSLA steel at four test temperature for four grain sizes. This has allowed a significant advance in the understanding of how low temperature affects the cyclic strain hardening exponent, β_c, since we can now model β_c in terms of the separate athermal and thermal components of the flow stress. In addition, we have finished the work on cleavage characterization of Fe-binary systems which allows a determination of how alloying elements affect the specific work of fracture and in turn how this affects the ductile-brittle transition. Together, these allow a major step towards understanding how secondary modes of fracture affect the low temperature fatigue process in BCC systems. Over the last year, two graduate students (Rex King and James Lucas) have been involved in this phase of the research.

II-1: Cyclic stress-strain of HSLA steels.

James Lucas and William W. Gerberich

Cyclic plastic deformation data for a particular metal or alloy system is readily available in the literature.[1] However, fewer studies can be found which relate cyclic deformation parameters, such as β_c to consistent variations of microstructure, (e.g., grain size) within an alloy system. One exception is Yokobori et al[2] who have studied the dependence of β_c on the ferrite grain size in a low alloy steel at room temperature only. As far as could be ascertained from the literature, there have been no simultaneous studies of grain size and low temperature effects on the cyclic fatigue properties of low alloy steel. Thus, the aim of this ongoing work is to provide information, from

which structure-property relationships for β_c can be established. The ultimate goal is to incorporate these data into a model for low temperature fatigue crack propagation near and at threshold. In this investigation grain size and temperature effects on the cyclic strain hardening, β_c, were examined. The grain size effect will only be casually mentioned while the temperature effect will be discussed in more detail.

The material used was an HSLA steel with an as-received yield stress of 414 MPa. The major alloying elements were 0.06%C, 0.03% Nb and 0.35% Mn by weight. The desired grain sizes (10-123 μm) were acheived by soaking at 1473K for various time durations in vacuum at $<10^{-5}$ Torr, and then allowing to furnace cool. Test temperatures ranging from 123K to 300K were controlled to within ±1K by using a cold chamber which operates by circulating liquid nitrogen vapor through baffled-studded construction over heating elements.

Further details of cyclic fatigue testing and analysis are given in Appendix I.[3] The main result is that the saturated cyclic fatigue stress curves were essentially parallel for all grain sizes as indicated in Figures 1 (a, b, c), independent of test temperature. This suggested that cyclic strain-hardening rates could be interpreted in terms of a temperature independent athermal component, σ_i. The final result is that the cyclic strain hardening exponent (the log-log slope of the data in Figure 1) at any temperature, β_c, could be determined from the temperature independent value, β_{c_i}, through

$$\beta_c\,(0.002)^{-\beta_c} = \left[\frac{{\beta_c}^i\,K^i}{\sigma^* + \sigma_{i(0.002)}}\right]\left[\frac{\sigma_{i(0.002)}}{K^i}\right]^{1-\beta_c/{\beta_c}^i} \qquad \text{Eq. (4) Appendix I}$$

Since σ^* is the thermal component of the flow stress which may be predicted in terms of the Dorn-Rajnak theory as a function of temperature and alloying elements[4] and since ${\beta_c}^i$, K^i and σ_i are temperature independent, it is now possible to predict β_c for any temperature below room temperature. Such a prediction from Eq. (4) is shown in Figure 2 to be very good.

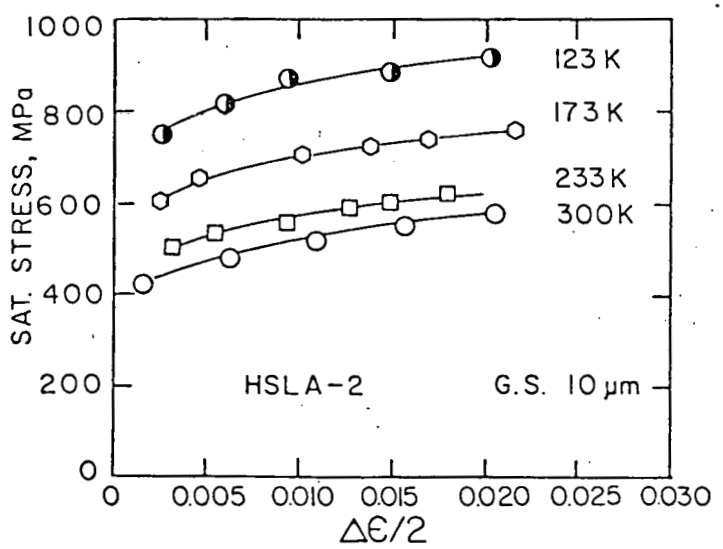

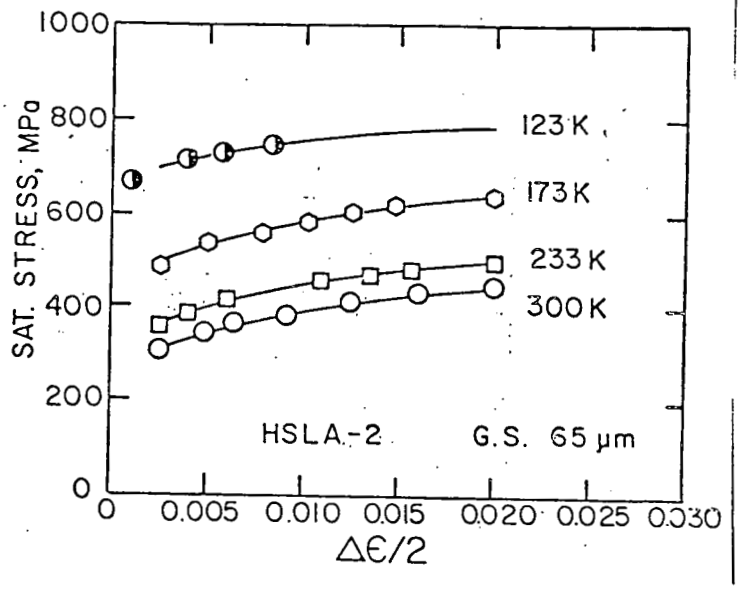

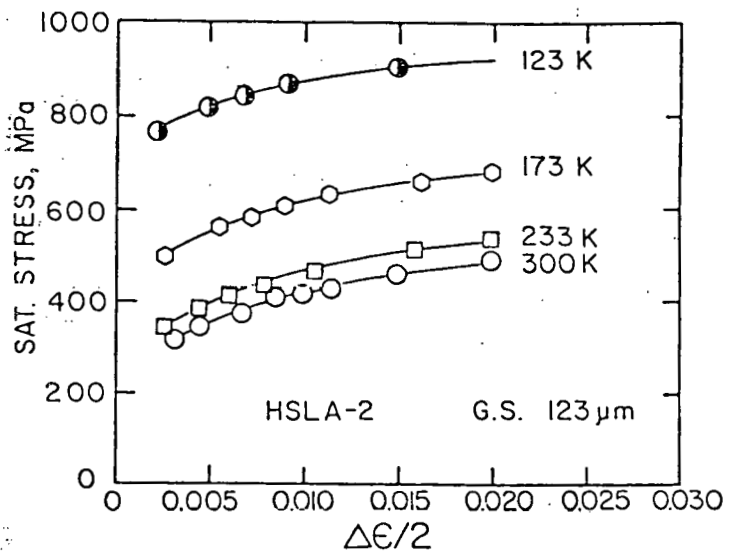

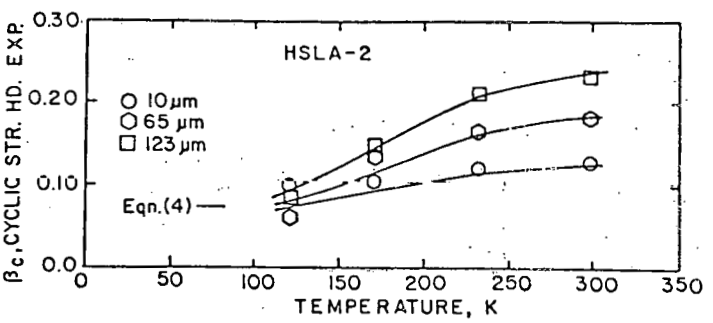

FIGS. 1 a, b, c
Cyclic saturation stress versus total strain amplitude. a) 10 μm, b) 65 μm, c) 123 μm grain sizes.

FIG. 2
Comparison of experimental and analytical results of the cyclic strain hardening exponent as a function of temperature at various grain sizes in an HSLA steel.

II-2 Burst cleavage in BCC Fe

W.W. Gerberich, Y.T. Chen, D.G. Atteridge and T. Johnson

Although not presently working on the project, three former associates, Dr. David G. Atteridge of Battelle Northwest Laboratories, Dr. Y.T. Chen of Pitney-Bowes Corporation and Mr. Tom Johnson of Chrysler Corporation have collaborated on this project. We now have a working model for those alloying and microstructural effects which control the ductile to brittle transition temperature, T_{DBTT}, in Fe and Fe-binary systems. Using twin or slip-band nucleated Ti(C,N) fracture as the triggering event for cleavage, the specific work of fracture for iron alloys was determined. For Fe-Si and Fe-Ni this is shown in Figure 3. Coupling this fracture mechanism with the previously determined flow model[4] enabled a predictive model to be given in terms of fundamental parameters by

$$T_{DBTT} = \frac{4\,\theta\Gamma_o^{\frac{1}{2}}\,b^2\left\{\sigma^*_{p_o} - \beta'\,\frac{\xi_m^2\,C}{b^3}\right\}\left\{\sigma^*_{p_o} + k_y d^{-\frac{1}{2}} - \frac{\xi_m^2\,C}{b^3}\left(\beta' - \frac{1}{kT_c}\right) - \frac{\sigma^*_f}{pcf}\right\}}{\pi^{3/2}\,k\{\ln(\dot{\varepsilon}_o/\dot{\varepsilon})\}\{\sigma^*_{p_o} - k_y d^{-\frac{1}{2}} - \frac{\xi_m^2\,C}{b^3}\left(\beta' + \frac{1}{kT_c}\right) + \frac{\sigma^*_f}{pcf}\}} \qquad \text{Eq. (14) Appendix II}$$

Here, the transition temperature is given by the dislocation line energy, Γ_o, the burgers vector, b, the misfit parameter, ξ_m, the solute concentration, C, the Peierls stress for pure Fe, $\sigma^*_{p_o}$, the Hall-Petch slope, k_y, the cleavage fracture stress, σ_f^*, and the plastic constraint factor, pcf, for a charpy bar. One comparison, as seen in Figure 4 is quite good for both the data of this investigation and several others. Details are given in Appendix II.[5]

References (Section II)

1. R.W. Landgraf, Work Hardening in Tension and Fatigue, ed. A. Thompson, TMS-AIME, Warrendale PA, p. 240, (1977).

2. T. Yokobori, H. Ishii and S. Kayama, Scripta Met. 13, p. 515 (1979).

3. J.P. Lucas and W.W. Gerberich, "Low Temperature and Grain Size Effects on the Cyclic Strain Hardening Exponent of an HSLA Steel," Accepted for publication, Scripta Met., (1981).

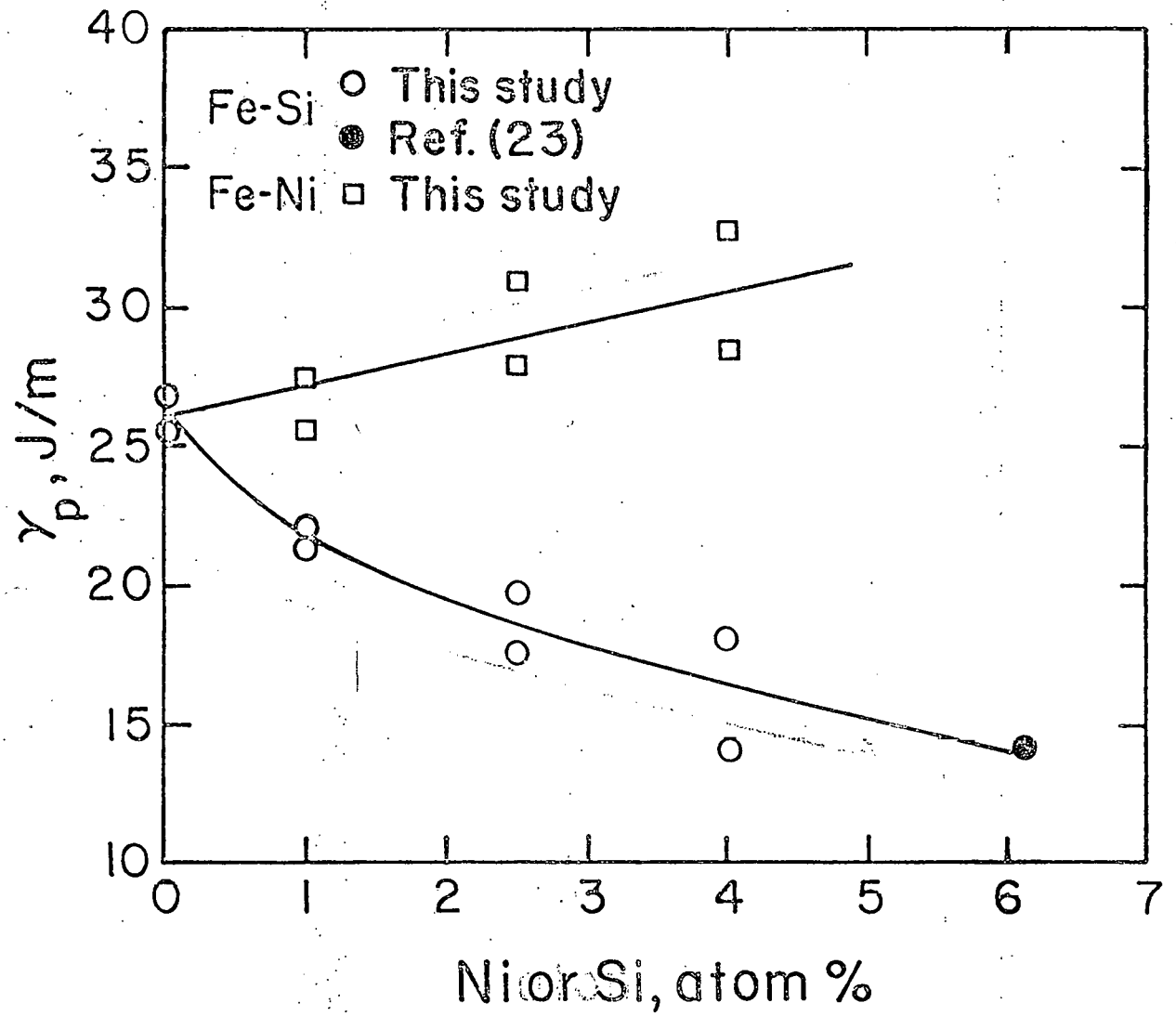
Fe-Si
This study
Ref. (23)
Fe-Ni
This study
γ_p, J/m
40
35
30
25
20
15
10
0
1
2
3
4
5
6
7
Ni or Si, atom %

Figure 3

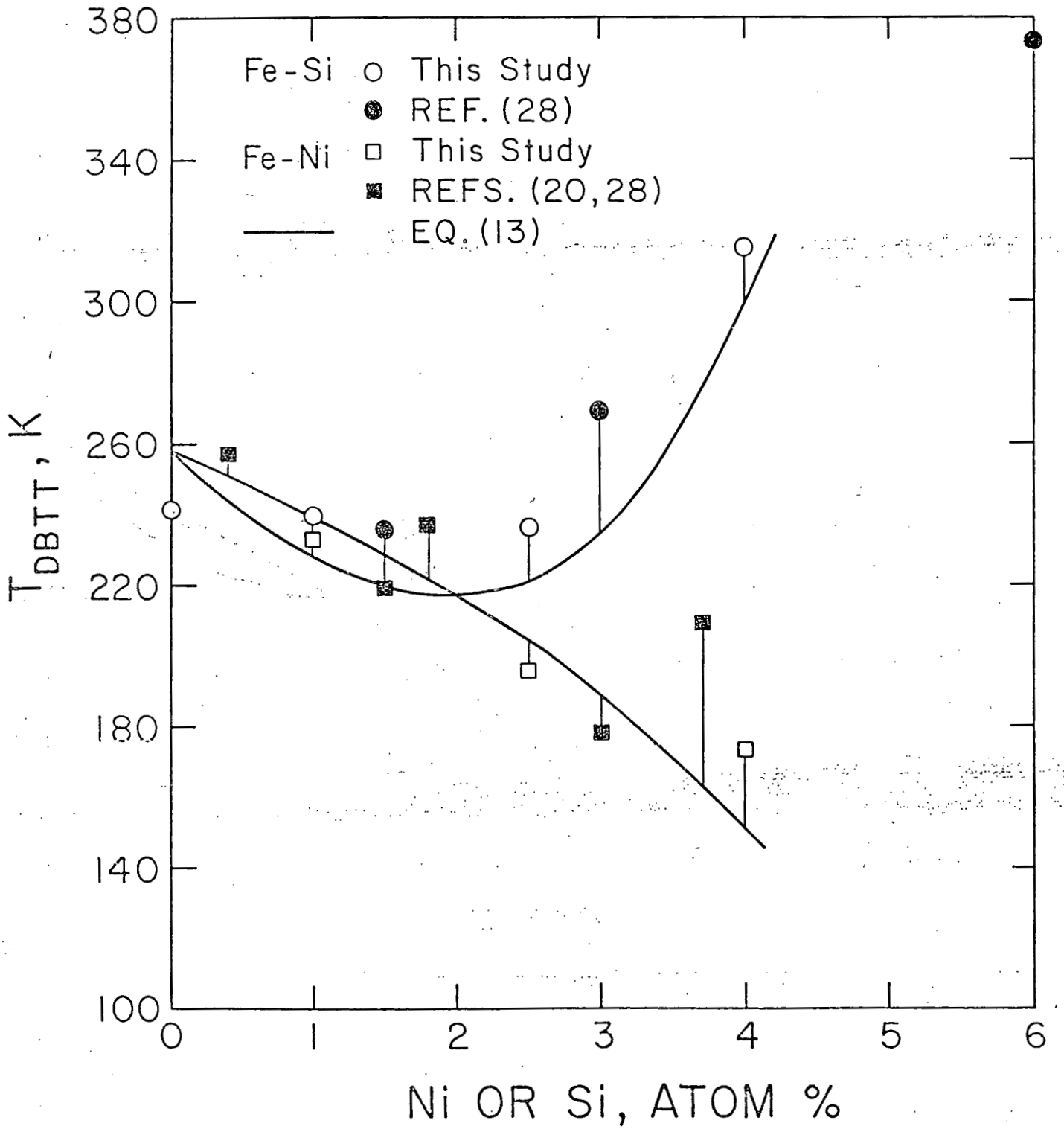
Fe-Si
This Study
REF. (28)
Fe-Ni
This Study
REFS. (20,28)
EQ. (13)
T_{DBTT}, K
380
340
300
260
220
180
140
100
0
1
2
3
4
5
6
Ni OR Si, ATOM %

Figure 4

4. Y.T. Chen, D.G. Atteridge and W.W. Gerberich, "Dislocation Dynamics of Fe-binary Alloys: I. Low Temperature Plastic Flow," accepted for publication, Acta Metallurgica, (1981).

5. W.W. Gerberich, Y.T. Chen, D.G. Atteridge and T. Johnson, "Dislocation Dynamics of Fe-binary Alloys: II. Application to the Ductile-Brittle Transition," ibid.

III. FATIGUE CRACK GROWTH

In the second year, emphasis has been in measuring fatigue crack propagation rates at low ΔK values near threshold. These measurements suggest that some of the initial ideas in the original proposal are correct and that some need revision. For example, Cyclic cleavage does control fatigue crack propagation rates in HSLA steel and Ti-30Mo at intermediate ΔK. We have made additional progress in both experimentally defining cyclic cleavage and theoretical modelling. Nearer threshold, the process seems to be controlled by a more ductile process. This is still in the definition stage and requires transmission microscopy of the crack-tip region. In addition, there have been several possible mechanisms recently proposed for threshold stress intensities including microcrack zones, crack bifurcation, crack-closure and crack-tip wedging phenomena. The complexity of the observations suggest that additional tests with environmental control and load-ratio variation are necessary for precise interpretation. Three students, James Lucas, Kumar Jatavallabhula and Chyun-Hua Chang, have been involved in this last year's effort.

III-1. Fatigue crack growth in HSLA steels

James Lucas and William W. Gerberich

Fatigue crack propagation studies covering three decades of growth rate near threshold have been completed for three grain sizes (10 μm, 65 μm, and 123 μm) at four test temperatures (123, 173, 233 and 300K). The results for the 65 μm grain size material are shown in Figure 1. First, it is seen that the highest temperature has the lowest threshold with a value of about 10 MPa-$m^{\frac{1}{2}}$ increasing to 15.5 MPa-$m^{\frac{1}{2}}$ at 123K. The very large increase in slope at about a ΔK of 17.5 MPa-$m^{\frac{1}{2}}$ is seen to increase drastically for the lowest temperature but more gradually for the highest test temperature. Similar behavior were observed for both the 10 μm and 123 μm grain size material.

The reason for the strong slope change in Figure 1 was associated mainly

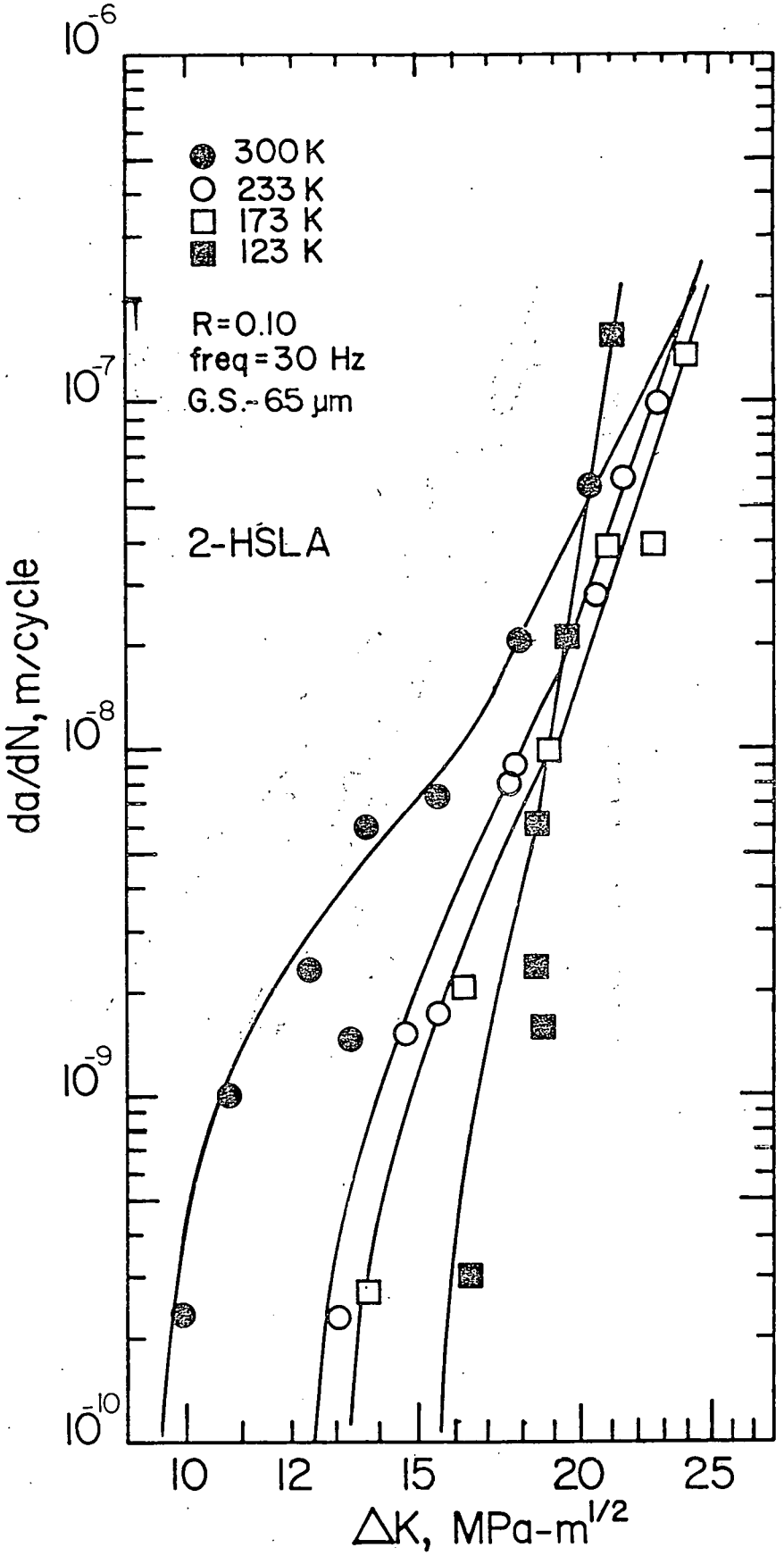
300 K
233 K
173 K
123 K
R=0.10
freq=30 Hz
G.S.-65 μm
2-HSLA
da/dN, m/cycle
ΔK, MPa-m^1/2
10^-6
10^-7
10^-8
10^-9
10^-10
10
12
15
20
25

Figure 1

with enhanced cyclic cleavage at low test temperatures. An example of this is shown in Figure 2(a) for a 123 μm grain size material tested at a ΔK of 20 MPa-$m^{\frac{1}{2}}$ where the macroscopic growth rate was 9.8×10^{-8} m/cycle. On the other hand, calculation of the growth rates from the finest microcleavage jogs indicates a value closer to 1.5×10^{-6} m/cycle or about a factor of fifteen enhancement. This cyclic cleavage enhancement over a more ductile growth process is similar to that observed for Fe-Ni and Fe-Si alloys.[1] The more nearly ductile process is shown in Figure 2(b) for the 123 μm grain size material at 123 K and was observed to be more predominant than the cyclic cleavage process at threshold. Here, the macroscopic growth rate of 3.2×10^{-10} m/cycle was on the order of three orders of magnitude slower than the apparent microscopic growth rate of $\approx 6 \times 10^{-7}$ m/cycle as observed by scanning microscopy. This suggests that the true ductile striation markings were beyond the SEM resolution or that there were relatively large waiting times between various grains growing along the crack front. Whatever the situation, it appears as though the ductile process is controlling near threshold.†

Data for other grain sizes at the same series of test temperatures are shown in Figure 3. It is seen that for this load ratio, R = 0.1, and a 30 Hz test frequency that there is an orderly progression of increasing thresholds with either decrease in test temperature or an increase in grain size. Anal-

† It is feasible that discontinuous growth by a ductile mechanism along the front arrests at much lower ΔK values. Here, it might be assumed that the ductile process can only connect together when a few selected grains fail by cyclic cleavage. This would be just enough to lower the resistance of the microcrack zone to the point where the remaining grains fail by a ductile or brittle process. In this context, 10 or 20 percent cyclic cleavage may be sufficient to trigger the onset of threshold.

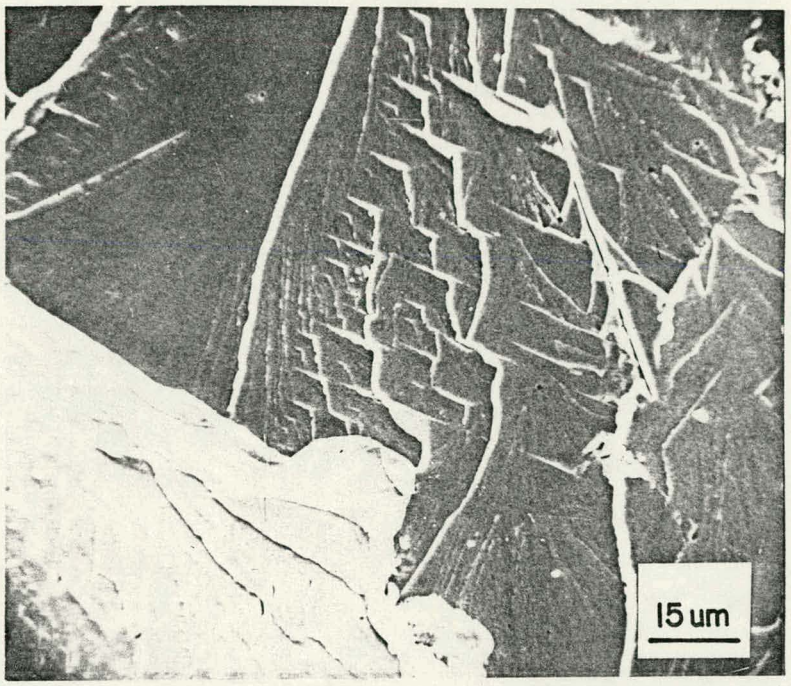

da/dN

(a) 123μm: T = 123 K; ΔK = 20 MPa-m$^{1/2}$

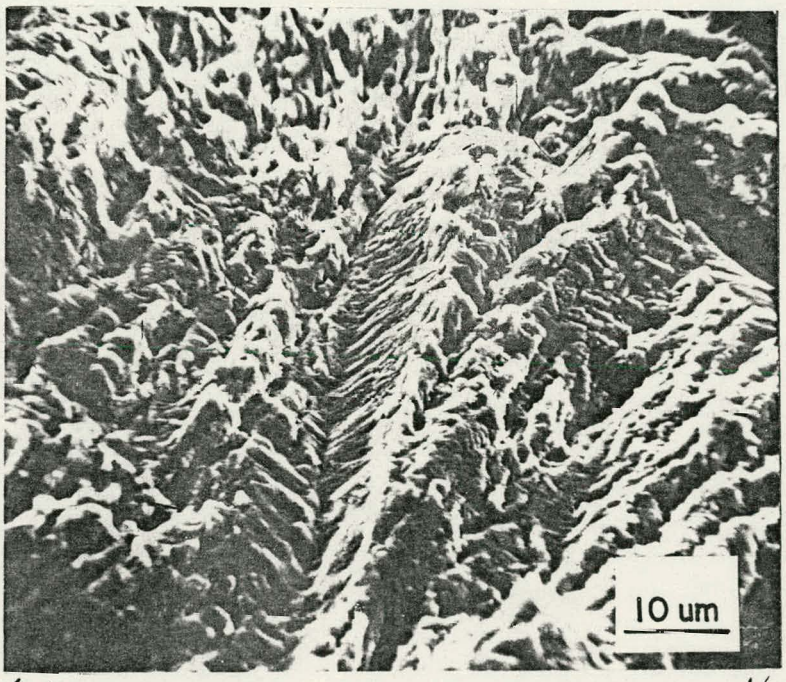

(b) 123μm: T = 123 K; ΔK = 18 MPa-m$^{1/2}$

Figure 2

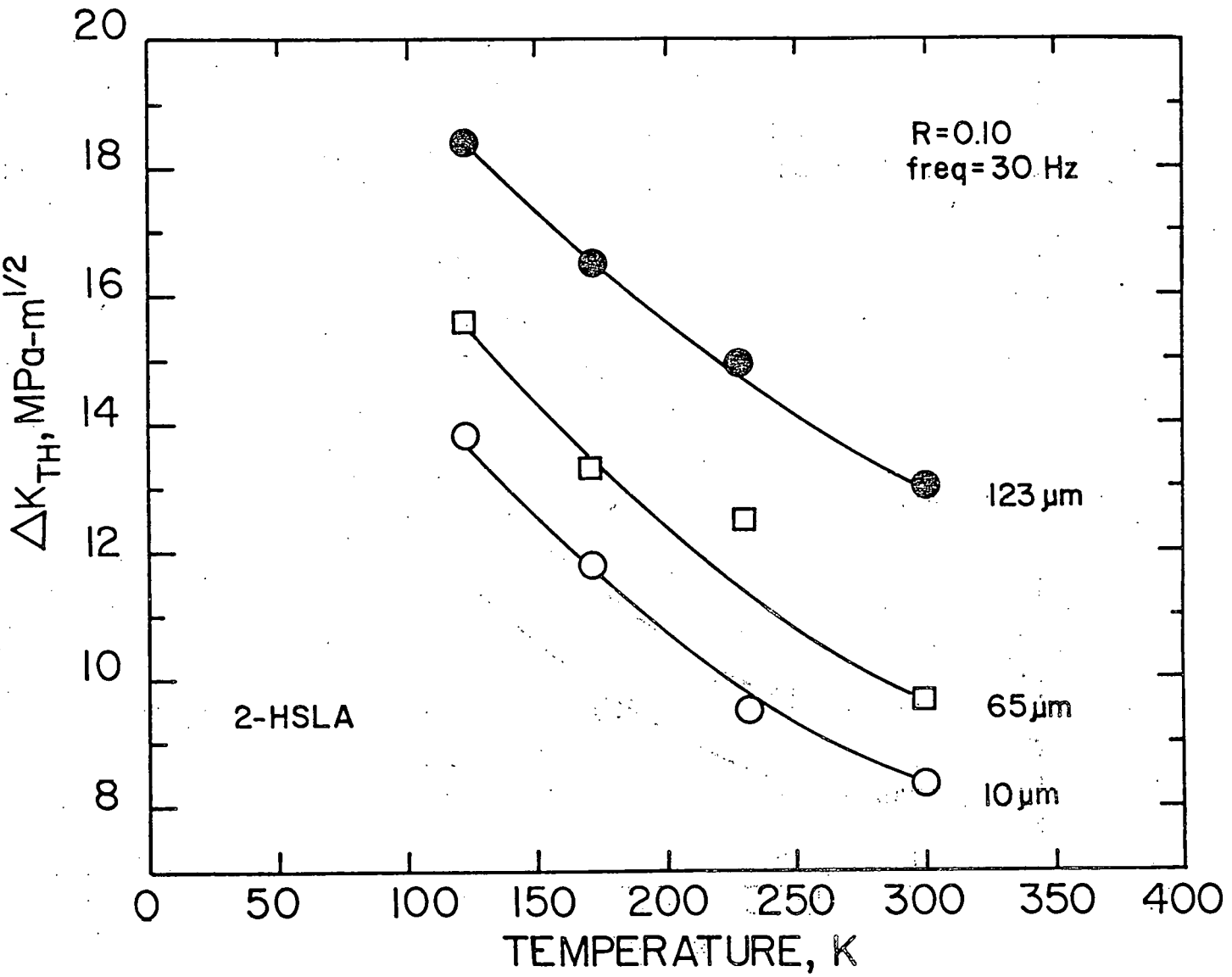
20
18
16
14
12
10
8
ΔK_{TH}, MPa-$m^{1/2}$
R=0.10
freq=30 Hz
123 μm
65 μm
10 μm
2-HSLA
0
50
100
150
200
250
300
350
400
TEMPERATURE, K

Figure 3

ysis of these threshold data were accomplished first by using two analyses as originally proposed. The first is a very simple concept in terms of the reversed plastic zone size ($R_{p\pm}$) as given by

$$\Delta K_{TH} = 6.14\ \sigma_{ys}\ \sqrt{d} \qquad (1)$$

where σ_{ys} is the yield strength and d is the average grain diameter. The second is in terms of a semi-cohesive zone model.[2] If a void fraction of $f_v \approx 0.3$ at the crack tip is due to cyclic plasticity and cleavage and a reversed, constrained, strain-hardened yield zone gives $\sigma_{ys\pm} \simeq 4\sigma_{ys}$, the results in Figure 4 seem to predict these data as a first approximation. A much better prediction model would be to base the analysis on a cyclically work-hardened flow stress since the cyclic hardening exponents, β_c, vary from 0.06 to 0.22. Since the highest data points in Figure 4 for a given grain size represent the lowest-test temperatures and hence the lowest β_c values, the upper point would move little to the right while the lower ones would move substantially by changing the abscissa to $\sigma_{flow}\sqrt{d}$. A demonstration of this follows.

Just as the plastic zone has been interpreted in terms of the ultimate strength, where there is a large spread between yield and ultimate, so can one use a flow stress determination under cyclic conditions, giving

$$\sigma_{flow} = \sigma_{ys}\left(\frac{\varepsilon\pm}{\varepsilon_{ys}}\right)^{\beta_c} \quad ; \quad R_{p\pm} \simeq \frac{\Delta K^2}{\pi(2\sigma_{flow})^2} \qquad (2)$$

If one then evaluates the flow stress at two percent cyclic strain and assumes the reversed plastic zone size at threshold is equal to the grain size, the prediction becomes

$$\Delta K_{TH} \simeq 3.54\ (10)^{\beta_c}\ \sigma_{ys}\sqrt{d} \qquad (3)$$

where $\varepsilon\pm/\varepsilon_{ys} = 10$. Taking the cyclic strain hardening exponent and the yield strength for each grain size and test temperature and calculating ΔK_{TH} from Eq. (3) gives a slightly better comparison to the threshold data from

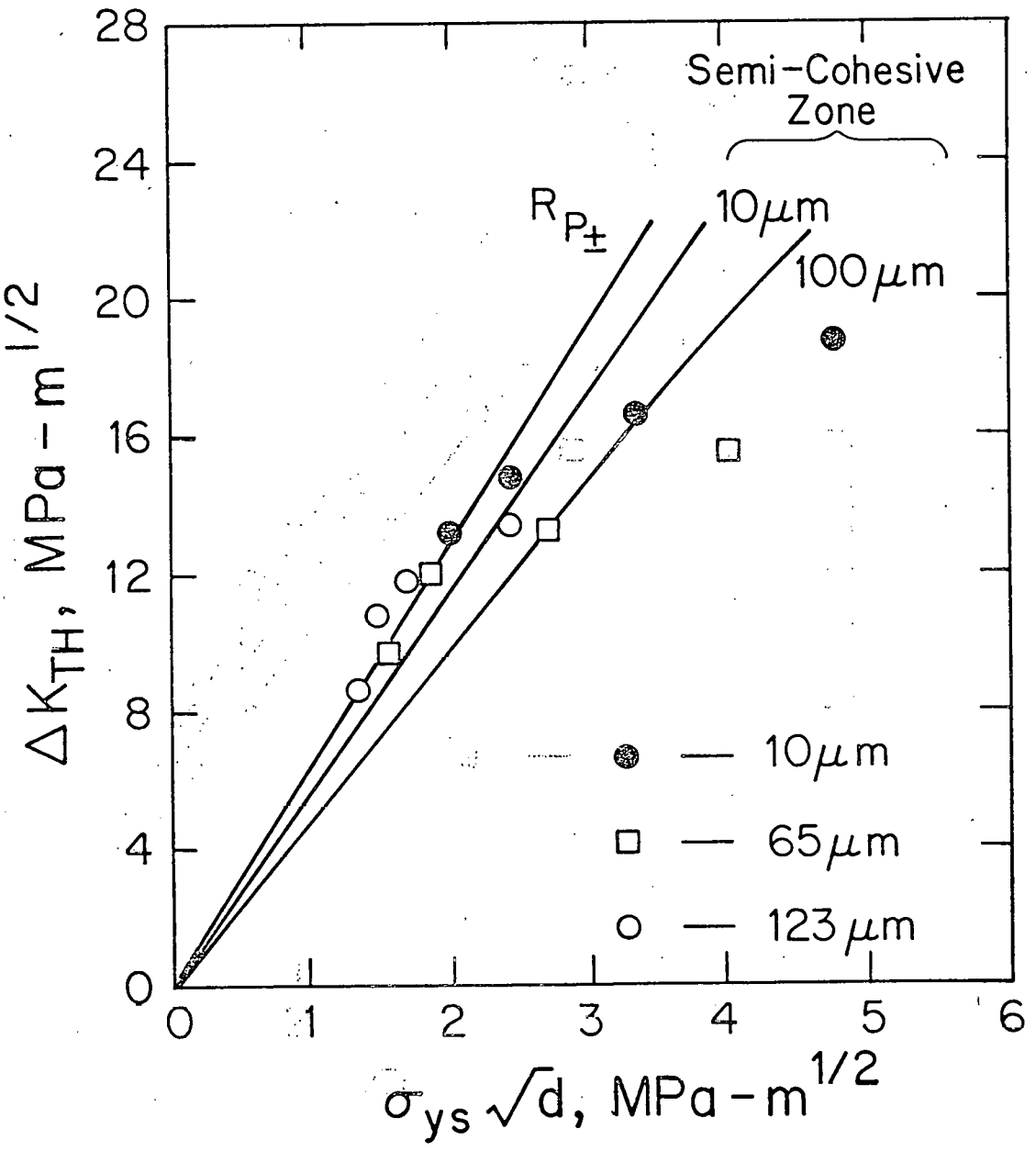
Semi-Cohesive Zone
$R_{P\pm}$
10μm
100μm
10μm
65μm
123μm
ΔK_{TH}, MPa-m$^{1/2}$
$\sigma_{ys}\sqrt{d}$, MPa-m$^{1/2}$
0
4
8
12
16
20
24
28
0
1
2
3
4
5
6

Figure 4

Figure 3 as seen in Figure 5. Even this needs refinement since nothing has been proposed with regards to strain rate sensitivity and the strain level of two percent at threshold is purely arbitrary. Since $\varepsilon_{ys} \approx 0.002$, this implies that the distance inside the grain which is significant is about one-tenth the grain diameter. Perhaps it is significant that the substructure of HSLA steel fatigued at 144 K did exhibit sub-cell structures[3] on the order of 1 μm which is about one-tenth of the grain diameter.

Further detailed substructural and theoretical analyses are in order to separate the various contributions and attempt to define the controlling mechanism(s).

III-2 Fatigue crack growth in model alloy Ti-30 Mo

Kumar Jatavallabhula and William W. Gerberich

In body-centered-cubic Ti-30 Mo, over three decades of fatigue crack growth rate have been studied in the threshold and Paris law regimes. For five test temperatures ranging from 123 to 340 K, threshold regime data are shown in Figure 6 for vacuum annealed samples with a grain size of 93 μm. Compared to the steel data, where thresholds changed by about 50 percent as the temperature was lowered by 177 K, the Ti-30 Mo data only changed by about 30 percent with an even greater 217 K decrease in temperature. Furthermore, the data are only orderly to 189 K with thresholds increasing with decreasing test temperature. Beyond that, there appears to be a decrease in threshold with a further decrease in test temperature. This corresponds to a fatigue ductile-brittle transition temperature with a greater tendency for cyclic cleavage to occur at temperatures below this transition temperature. If such behavior can be extrapolated to the steel data, then it would indicate that the ductile mechanism is controlling in the HSLA steel at all temperatures down to 123 K.

On the other hand, there are substantial differences in the cyclic cleavage appearance of the Ti-30 Mo suggesting that cyclic plasticity modelling

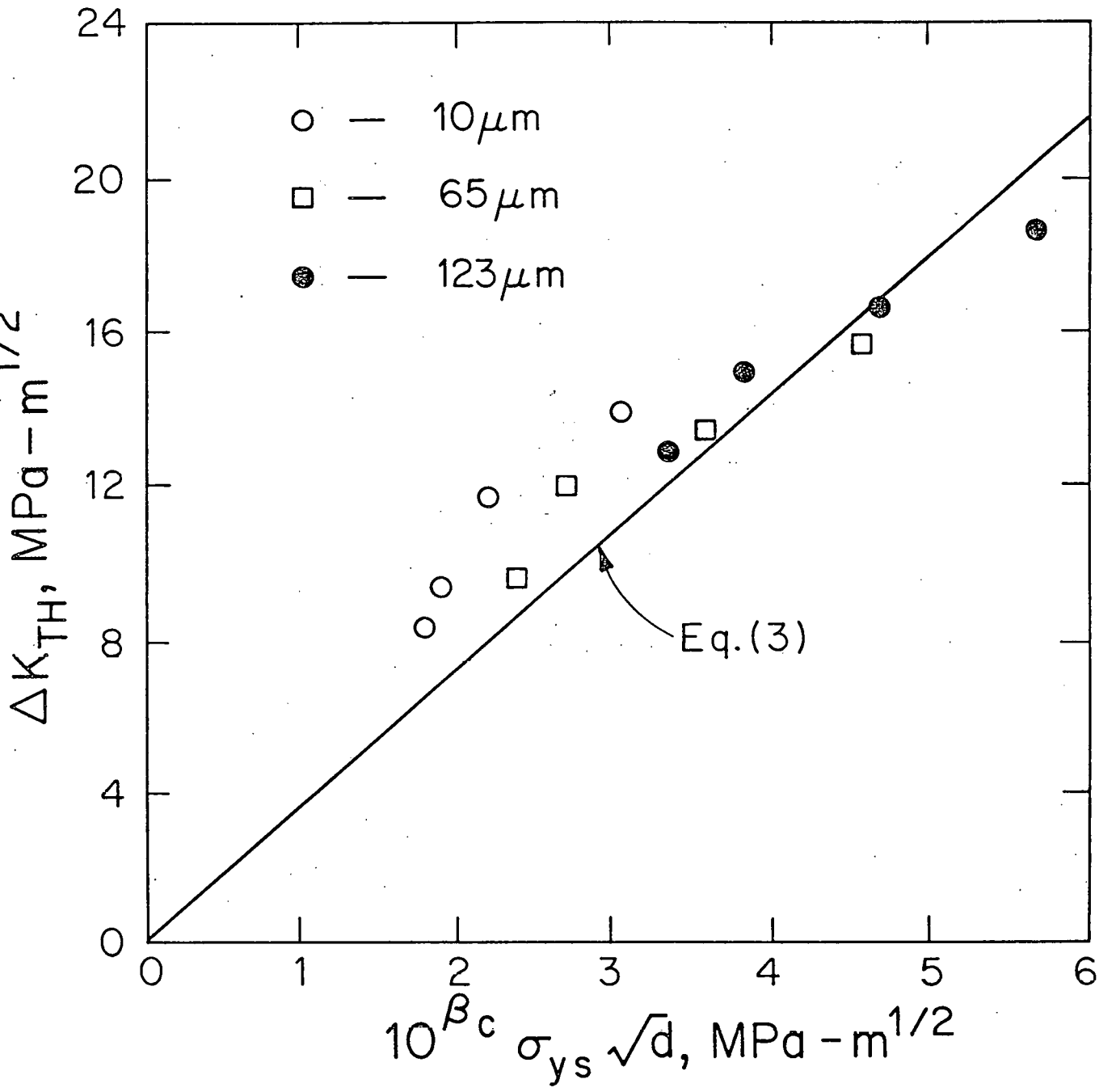
24
20
16
12
8
4
0
0
1
2
3
4
5
6
○ — 10μm
□ — 65μm
● — 123μm
Eq.(3)
ΔK_TH, MPa-m^1/2
10^βc σ_ys √d, MPa-m^1/2

Figure 5

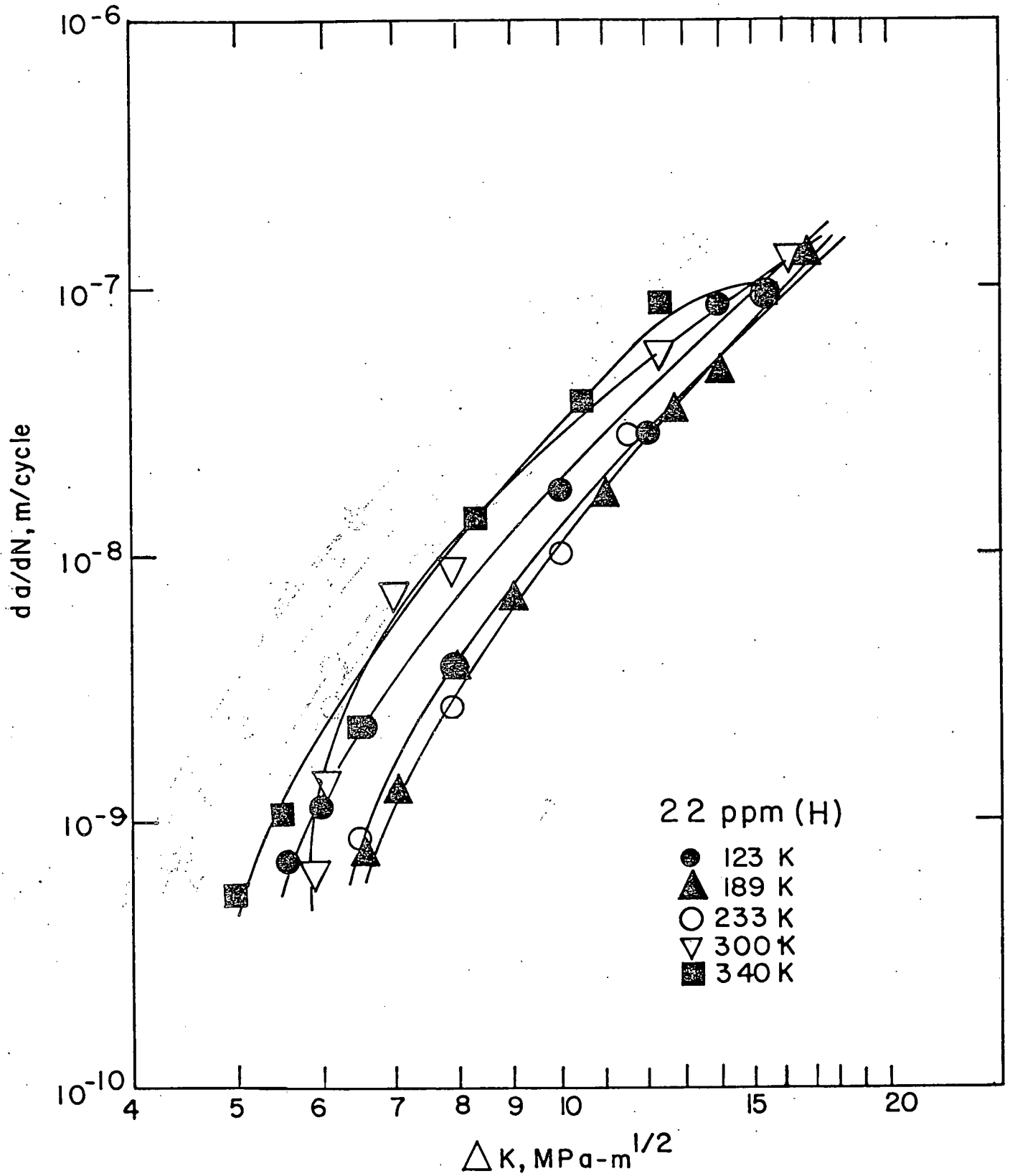
10-6
10-7
10-8
10-9
10-10
da/dN, m/cycle
4
5
6
7
8
9
10
15
20
ΔK, MPa-m1/2
22 ppm (H)
123 K
189 K
233 K
300 K
340 K

Figure 6

might be different for the two materials. For example, whereas the cyclic cleavage at 123 K under a ΔK of 20 Mpa-$m^{\frac{1}{2}}$ was relatively free of obvious plasticity in the steel, this was not always the case in Ti-30 Mo. The cyclic cleavage appearance in Figure 7(a) for a ΔK of 26 MPa-$m^{\frac{1}{2}}$ suggest little plasticity and gives a growth rate value roughly corresponding to the macroscopic observation; however, the "cyclic-cleavage" at a ΔK of 6 MPa-$m^{\frac{1}{2}}$ near threshold suggests considerable plasticity as seen in Figure 7(b). Such cyclic plasticity is clearly shown for the same alloy tested at 123 K (although now containing 1200 ppm hydrogen) in Figures 7(c) and (d). Here, there are multiple slip bands along each cyclic cleavage step with approximately five slip bands spaced at 0.4 μm along each cleavage advance. Following a previous analysis[1] of the crack opening displacement associated with such slip bands, the minimum required number of dislocations along n_R rivers would be

$$\delta_c = \frac{\Delta K^2(1-\nu^2)}{\pi \sigma_{ys} E} \leq n_R \bar{h} = n_R \bar{N} b \qquad (4)$$

where $\bar{N}$ is the number along each river, b is the burgers vector, ΔK is the cyclic stress intensity, σ_{ys} is the yield strength and E is the modulus of elasticity. These $\bar{N}$ dislocations may be divided into the number of slip bands along a single cleavage advance giving

$$\bar{N} = n_s \bar{N}_s \qquad (5)$$

where n_s is the number of slip bands per advance and $\bar{N}_s$ is the average number of dislocations in each slip band. If the dislocations can radiate out as an arrary from a point source, then $\bar{N}_s$ can be given in terms of the maximum distance the dislocation move, σ_{max}, and the density emitted, ρ_E. The maximum distance should be half of the spacing between rivers or, from Figure 7(c), about 2.1 μm. This may be used with

$$\bar{N} = n_s \pi r_{max}^2 \rho_E \qquad (6)$$

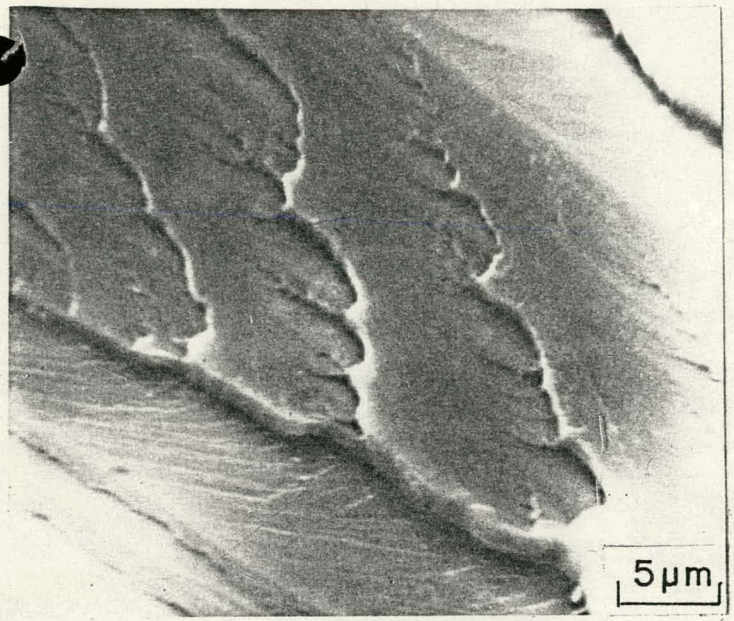

(a) 22 ppm: T = 123K;
ΔK = 26 MPa-$m^{1/2}$

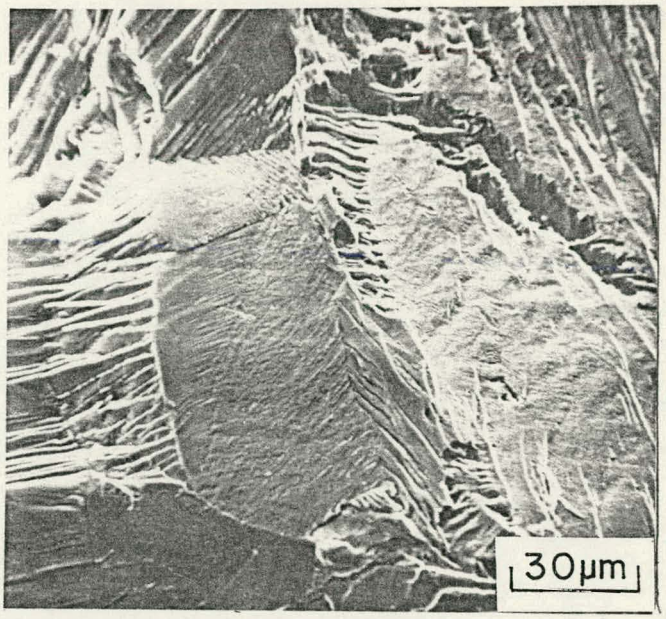

(b) 22ppm: T = 123K;
ΔK = 6MPa-$m^{1/2}$

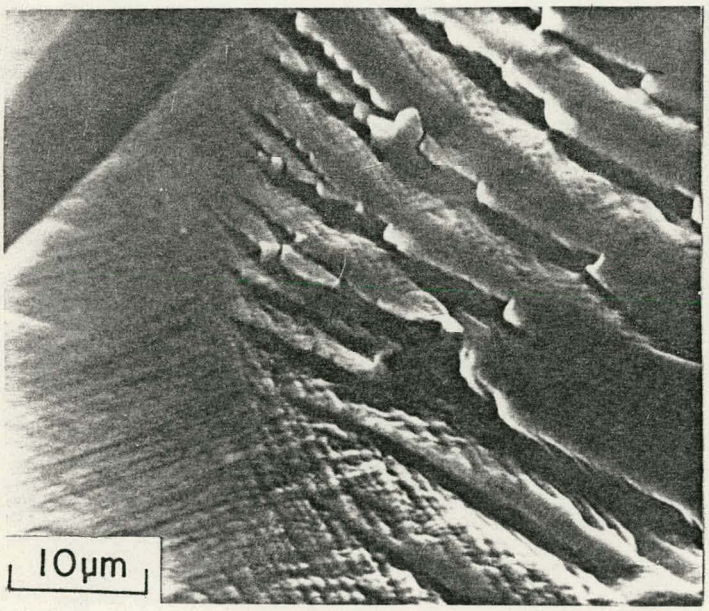

(c) 1200 ppm: T = 123K;
ΔK = 15.8 MPa-$m^{1/2}$

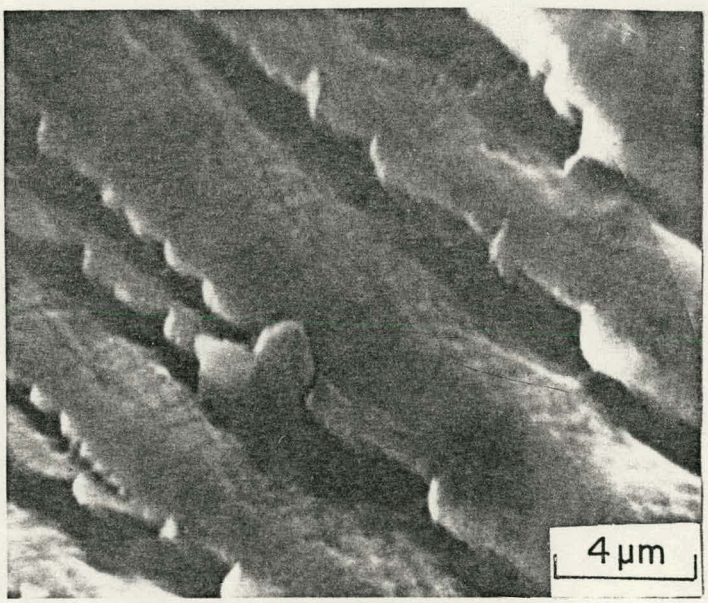

(d) same as (c)

Figure 7

and Eq. (4) for the 12 rivers observed in Figure 7(c) to find a $\rho_E \geq 2.1 \times 10^{12}/m^2$. However, this only requires three dislocations emitted into each slip band over the distance of 2.1 μm. The reason this is so small is that the calculation has ignored the fact that there is a severe twist angle and that additional step height accomodation is necessary. In turn, this requires a greater emitted dislocation density. This can be determined recognizing that

$$\delta_c + \delta_\psi = n_R \bar{h} \tag{7}$$

where δ_ψ is the twist angle displacement accomodation. Since $\bar{h}$ is on the order of 0.8 μm in height, it follows that the actual accomodation ($n_R\bar{h} = 9.6 \times 10^{-6}$m) is much greater than that required for crack-opening displacement alone ($\delta_c = 4.6 \times 10^{-7}$m). This revises the dislocation density required to $4.4 \times 10^{13}/m^2$, a realistic value. Furthermore, it now means that there would be 24 dislocations in the average emitted pile-up. This is more realistic but still probably not the best estimate since it is not specific with regards to how many slip systems are operating. If one examines the slip traces in Figure 7, there are probably two main sets of either {110}, {112} or {110}/{$\bar{1}$21} which could give intersection angles of 73.2 to 90°. Considering only orthogonal slip systems, with the arrary spaced along the cleavage step height the same as it is spaced along the rivers, one obtains 250 dislocations emitted into a single band. Clearly, before we can do this kind of accounting accurately, both the dislocation dynamics and thin film TEM observations of cyclically produced substructures must be assessed.

Finally, in the Paris law regime, the very low slope in Figure 8 for 300 K data only gives an exponent of 1.5 for $\partial \ell n(da/dN)/\partial \ell n \Delta K$. This is a lower ΔK dependence than might be expected for some cyclic plasticity models where a 2 to 4 dependence is common. Although the mechanism is cyclic plasticity at 300 K, it changes mainly to cyclic cleavage at 123 K. This later process gives rise to the large amount of scatter seen in Figure 8 for the 123 K data.

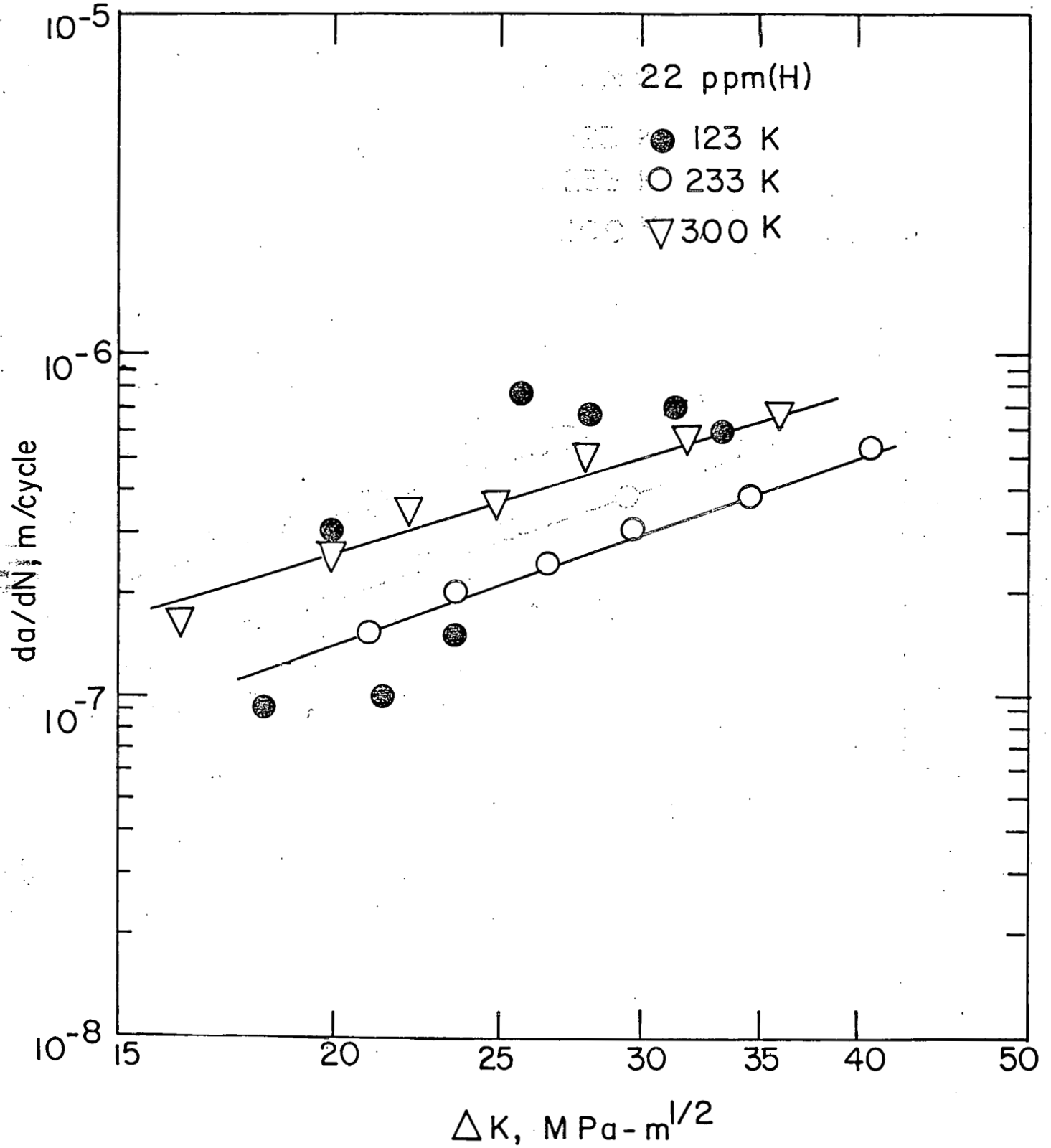
22 ppm(H)
123 K
233 K
300 K
10^{-5}
10^{-6}
10^{-7}
10^{-8}
da/dN; m/cycle
15
20
25
30
35
40
50
ΔK, MPa-$m^{1/2}$

Figure 8

Nevertheless, the increase in da/dN over the stress intensity range of 15 to to MPa-$m^{\frac{1}{2}}$ is seen to be less than an order of magnitude. This is in striking contrast to the three order of magnitude increase observed for HSLA steel at 123 K over a much smaller stress intensity range. In fact, the power-law exponent for these two materials changes from about 3.5 for Ti-30 Mo to 25 for steel even though the mechanism is basically cyclic cleavage in the vicinity of 10^{-7} m/cycle growth rate. This says that a basically different dislocation and/or strain-rate sensitivity response in these two materials exists at 123 K. These different responses lead to a different degree of sensitivity to cyclic cleavage.

Examination of this premise was possible with existing strain rate sensitivity data. In the previous technical report, we had reported that m^* $\simeq$ 17.5 for HSLA steel at 150 K. This corresponds to the Fe-Ti-C alloy previously evaluated which gave m^* values of 18 and 28.5 at 173 and 123 K. Extrapolating the HSLA steel data would give an m^* value near 22 at 123 K. On the other hand, the value for Ti-30 Mo at 123 K was reported as 42. This factor of two difference in m^* should actually produce lower slopes of da/dN versus ΔK for the steel while, in fact, the opposite is true. This is partly due to the approximate nature of theoretical model but, more interestingly, due to an important difference in the internal stress states when comparing Ti-30 Mo to HSLA steel. It may be recalled that the internal stress state at low temperatures for HSLA steel did decay and, after long time stress relaxation, did tend toward the higher temperature internal stress state. No such trend was observed for vacuum annealed Ti-30 Mo. Contrary to almost all other materials evaluated by these techniques, this material demonstrated the same internal stress after twelve hours of high-stress relaxation as it did after instantaneous unloading. This implies that the backward extrapolation technique for σ_i is in error and hence the previous m^* values would be meaningless. In fact, determination of m^* at 173 K from stress relaxation data gave a

value of eight rather than the value of 32 previously reported. If this factor of four difference also applies at 123 K, then the relative slopes predicted by strain-rate sensitivity arguments are much more in line with observation.

Still, it does not explain why the internal stress, rate sensitivity and concommittant fatigue-crack response in these two BCC alloys of comparable grain size and strength behave so differently. This will be a subject of next year's proposed work.

References (Section III)

1. W.W. Gerberich, N.R. Moody and K. Jatavallabhula, "A Proposed Cyclic Cleavage Crack Growth Model for Fatigue of BCC Iron and its Alloys," Scripta Metallurgica, 14 (1980) pp. 113-118.

2. W.W. Gerberich and N.R. Moody, "A Review of Fatigue Fracture Topology Effects on Threshold and Growth Mechanisms," Fatigue Mechanisms, Proc. ASTM-NBS-NSF Symp., J.T. Fong, ed., ASTM STP 675, Am. Soc. for Test. and Mat'ls, 1979, pp. 292-341.

3. M.R. Krishnadev and R. Ghosh, "Low-Temperature Mechanical Behavior of an "Acicular" Ferrite HSLA (High Strength-Low Alloy) Line Pipe Steel," Met. Trans. A, 10A, (1979) pp. 1941-1944.